Catalysis Today 148 (2009) 75–80

Contents lists available at ScienceDirect

Catalysis Today

journal homepage: www.elsevier.com/locate/cattod

Adsorption/desorption of NOx on MnO_2/ZrO_2 oxides prepared in reverse microemulsions

W.B. Li [a,b,*], X.F. Yang [b], L.F. Chen [c], J.A. Wang [c,**]

[a] Graduate School at Shenzhen, Tsinghua University, Shenzhen 518055, PR China
[b] Department of Environmental Science and Engineering, Tsinghua University, Beijing 100084, PR China
[c] Escuela Superior de Ingeniería Química e Industrias Extractivas, Instituto Politécnico Nacional, Col. Zacatenco, 07738 Mexico City, Mexico

ARTICLE INFO

Article history:
Available online 29 April 2009

Keywords:
NOx
Adsorption
Manganese oxide
Zirconia
Microemulsion

ABSTRACT

A series of MnO_2/ZrO_2 mixed oxides were prepared in reverse microemulsions for NOx adsorption and abatement. The results show that the amount of NOx adsorbed was increased with increasing MnO_2 content in various MnO_2/ZrO_2 samples. The maximum uptake value of NOx was 27.66 mg NOx/g adsorbent on the 40% Mn–Zr sample at 200 °C with NOx initial adsorption rate as 2.63 mg/(g adsorbent min). TPD results show that the complete desorption of NOx was easily obtained by heating the sample to 450 °C, and the temperature for the complete desorption can be further decreased to 210 °C by adding carbon monoxide into the argon desorption streams. Furthermore, water vapor was found to reduce NOx adsorption capacity because of its stronger competitive adsorption with NOx species. It is noteworthy that a small amount of sulfur dioxide could significantly increase the initial rate of NOx adsorption although it slightly decreased the NOx adsorption capacity.

1. Introduction

Among all the identified air pollutants, NO and NO_2, which are usually jointly referred to as NOx, are mostly formed during combustion of fossil fuels in both stationary and mobile sources including vehicles, airplanes, power stations, nitric acid plants as well as other industrial and domestic applications. NOx can contribute significantly to acid precipitation or urban photochemical smog. Selective catalytic reduction (SCR) of NOx with NH_3 on titania-supported V_2O_5 is the only effective technique to control the NOx emissions from stationary sources in the presence of excess oxygen [1], but these catalysts are expensive; moreover the exhaust gases usually need to be heated to meet the optimum catalyst operation [2]. On the other hand, three-way catalysts (TWCs) are commercially used to simultaneous removal of NOx, CO and hydrocarbons from the exhaust gases of automobiles operating at a point close to a stoichiometric mixture of air and fuel [3]. However, besides the high cost concerns, such Pt–Rh-based TWCs are ineffective for removal of NOx in the oxidizing exhaust gases from the lean burn engines that are developed in terms of the improved fuel economy [4]. Since the work by Iwamoto and Hamada [5], NOx reduction by hydrocarbons has been widely investigated in an effort to purify lean burn engine exhaust emissions [6], however, the catalysts still need to be improved regarding their hydrothermal stability and sulfur resistance ability [7,8].

Besides the SCR with ammonia or hydrocarbons, adsorption of NOx provides an alternative route for abatement of NOx in the presence of oxygen [4,9], which is carried out by first adsorbing NOx and then desorbing it by temperature swing or pressure swing techniques. These NOx adsorbent materials, usually consisting of precious metal (Pt) and alkaline earth metal (Ba) on an Al_2O_3 support, can store NOx in a nitrate form (typically, barium nitrate) during the lean cycle and release the stored nitrates during a subsequent fuel-rich cycle [10]. However, these materials have shown serious deactivation in the presence of SO_2 [11,12], due to the formation of stable sulfates, which block storage sites [10,13–16]. In addition, it is found that H_2O has a great effect on the NOx storage process, but is limited mainly at low temperatures (below 300 °C) [17].

The Ba-based oxide materials such as YBa_2Cu_3Oy, Ba–Cu–O, Ba–Al_2O_3, and Pt–Ba–Al_2O_3 were reported to have large NOx adsorption capacity [4,18–20], but they suffered from coexisting CO_2 because of strong adsorption of CO_2 on alkaline sites of these samples [21,22]. It has been reported that CO_2 negatively affects

* Corresponding author at: Graduate School at Shenzhen, Tsinghua University, Shenzhen 518055, PR China. Tel.: +86 755 26036729.
** Corresponding author. Tel.: +52 55 57296000x55261; fax: +52 55 55862728.
E-mail addresses: wblichem@yahoo.com.cn, wbli@mail.tsinghua.edu.cn (W.B. Li), jwang@ipn.mx (J.A. Wang).

0920-5861/$ – see front matter © 2009 Elsevier B.V. All rights reserved.
doi:10.1016/j.cattod.2009.03.028

the NOx storage process [10,17,23], whereas CO_2 has a promoting effect on NOx release in the fuel-rich phase [17,24,25].

Corbos et al. [26] recently reported that the inhibiting effect of CO_2 on the NOx uptake generally increased with the catalyst basicity (support = Al_2O_3, SiO_2, Al_2O_3–SiO_2 and $Ce_{0.7}Zr_{0.3}O_2$), indicating that the support was playing an important role in the effect of CO_2 on the NOx uptake. Similarly, Piacentini et al. [27] reported the dependence of NOx storage efficiency of Pt–Ba supported samples on various supports such as Al_2O_3, CeO_2, ZrO_2 and SiO_2, in 5 vol.% O_2/He at 300 °C.

In addition, various supports other than Al_2O_3 have been tested for NOx adsorption in the presence of CO_2 or SO_2. Palomares et al. [28] claimed that cobalt/copper hydrotalcites showed a high NOx storage capacity even in presence of SO_2 and water; Mn–Zr mixed oxides and Pt–ZrO_2–Al_2O_3 were reported to be able to resistant to CO_2 [29,30], because zirconia was basic enough to form stable nitrates on the surface whereas the carbonates were not produced on MnOx–ZrO_2 and Pt–ZrO_2–Al_2O_3 systems in dynamic conditions as suggested by Eguchi et al. [30] who reported that the Mn–Zr mixed oxides prepared by co-precipitation method could adsorb 0.406 mmol NO/g adsorbent in 6 h and 0.268 mmol NO/g adsorbent in 1 h on MnOx–ZrO_2 and 1 wt% Pt–5 wt% ZrO_2–Al_2O_3, respectively. The high NOx adsorption capacity could be achieved on Ce modified CuO/TiO_2 without deactivation by CO_2 [31], the authors also implied that pore structures and surface areas were playing key roles in the control of NOx adsorption capacity and adsorption rate [32]. On the other hand, the microemulsion method was very effective to control particle sizes and surface area of the metal oxides compared to the conventional precipitation method [33], which can provide a better dispersion of active metal components on their surface and facilitate diffusion of NOx inside the pore structures of samples.

In this paper, the MnO_2/ZrO_2 mixed oxides with high surface areas were prepared through a reverse microemulsion approach, with the aim to improve the amount of NOx uptake. NOx adsorption on such MnO_2/ZrO_2 samples was studied as compared to the similar samples prepared by co-precipitation method. In addition, regeneration of NOx adsorbents and effects of sulfur species and water vapor on NOx adsorption were also investigated.

2. Materials and methods

2.1. Preparation and characterization of MnO_2/ZrO_2 samples

Two aliquots of reverse microemulsions of H_2O/Triton X-100/n-hexanol/cyclohexane with the identical molar ratio as 16.2:1:6.3:43.1 were first prepared, of which one contained an appropriate amount of 25 wt% aqueous hydrous ammonia and the other contained a mixed aqueous solution of zirconyl chloride and manganese nitrate. They were thoroughly mixed and stirred for 1 h, thereafter the precipitates were obtained after distilling for 2 h, followed by filtering and washing with ethanol and water to eliminate excess organic species and chloride ions. The white powders were then obtained after drying at 100 °C in air and calcining at 450 °C in oxygen. The sample was denoted as *x*% MnZr, where *x* is molar ratio of MnO_2 to ZrO_2 in the samples. For a reference, a MnO_2/ZrO_2 mixed oxide sample was also prepared in a co-precipitation procedure where zirconyl chloride and manganese nitrate were the zirconium and manganese precursors and $NH_3 \cdot H_2O$ was precipitant. This MnO_2/ZrO_2 sample containing 40 mol% MnO_2 was denoted as 40% MnZr-CP.

Nitrogen adsorption and desorption isotherms were measured at −196 °C on Quantachrome Autosorb-1 Analyzer after the sample was outgassed at 450 °C for 12 h, and the specific surface area was calculated by the BET method and the pore size distribution of the sample was determined using the procedure proposed by Barrett, Joyner and Halenda (BJH). Powder X-ray diffraction (XRD) patterns were recorded on a Rigaku D/max RB X-ray diffractometer using nickel-filtered Cu Kα (λ = 0.15404 nm) radiation. The step scans were taken over the range of 2θ angles from 20° to 70° in steps of 0.02°, the intensity data for each step being collected for 5 s.

2.2. NOx adsorption and desorption measurements

NOx adsorption measurement was carried out on a thermogravitric analysis apparatus (Thermal Analyst 2000) in a fluidized system. The inlet gases containing 2000 ppm NO, 5% O_2 and with N_2 as balance were passed over the 50 mg sample with a flow rate 100 ml/min. The weight gain/loss on the sample was continuously monitored with thermogravimetric analysis.

Temperature programmed desorption (TPD) tests were conducted in a fixed bed reactor. The effluent gas was analyzed by a NO–NOx Chemiluminescence Analyzer (Thermal Electronics Model 42CHL). The sample (100 mg) was first pretreated in argon by heating from room temperature to 450 °C and holding at 450 °C for 2 h to remove any impurities adsorbed on the surface, then cooled down to 100 °C in argon. Subsequently, the adsorption measurement was carried out by exposing the sample to 2000 ppm NO and 2% O_2 at 200 °C until the adsorption amount of NOx on the sample reached its saturation capacity. Thereafter the sample was heated between 200 °C and 600 °C at a constant temperature sweep rate of 10 °C/min in a stream of argon with or without 0.6% CO at a total flow rate of 100 ml/min. The desorbed gas effluent of NOx and NO was continously recorded.

3. Results and discussion

3.1. Characterization of the MnO_2/ZrO_2 samples

The pore structure of the 15% MnZr sample derived from the N_2 adsorption/desorption isotherm is shown in Fig. 1. The adsorption/desorption loop at relative pressure (p/p_0) of 0.6–0.8 indicates the mesostructural texture of the sample. The pore size distribution calculated from BJH equation is centered at 5.7 nm as shown in Fig. 1.

Thermal stability is always a practical concern for the NOx adsorbent materials. Fig. 2 shows the XRD patterns of the obtained 15% MnZr calcined at different temperatures. The result indicates that the 15% MnZr was amorphous at 450 °C, and it transformed to a tetragonal phase (2θ = 30.2°) at 600 °C as confirmed by the broad XRD peaks due to the small crystallite sizes in the sample, and then a mixture of tetragonal and monoclinic (2θ = 28.2° and 2θ = 31.5°) modifications appeared at 900 °C. Generally, there are three

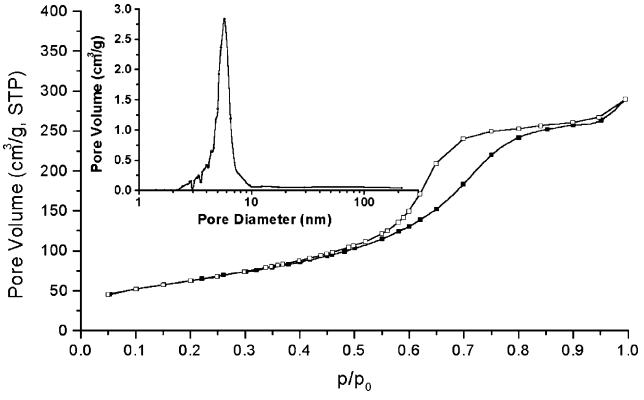

Fig. 1. Nitrogen adsorption/desorption isotherms and pore size distribution from the BJH equation of 15% MnO_2/ZrO_2 calcined at 450 °C.

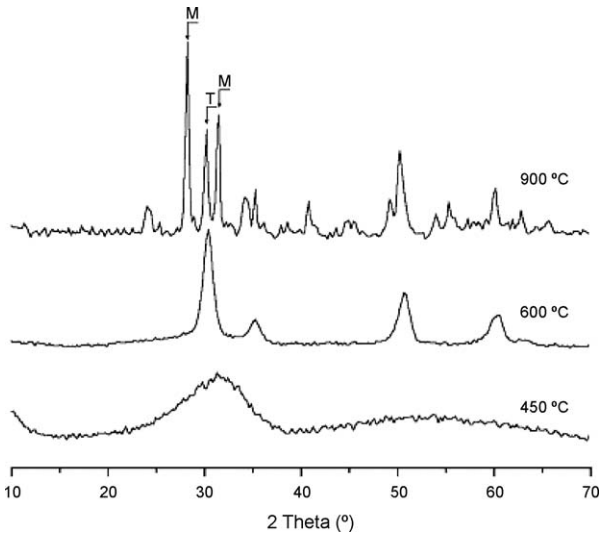

Fig. 2. XRD patterns of 15% MnO_2/ZrO_2 calcined at the different temperatures: M, monoclinic phase; T, tetragonal phase.

crystalline phases, i.e., tetragonal, monoclinic and cubic modifications for zirconia [34]. Here, it was demonstrated that addition of MnO_2 could help to stabilize the tetragonal crystalline structure below 600 °C, which may facilitate the adsorption of NOx on the sample under practical conditions such as in hot combustion gas purification [31].

3.2. NOx adsorption/desorption on the MnO_2/ZrO_2 samples

The widely investigated NOx storage material generally consists of precious metals and alkaline earth metal oxides as the NOx storage carriers, and a metal oxide, i.e., alumina, as support [10]. Many investigations were carried out to optimize these three components to obtain high NOx storage performance. Here NOx adsorption on the various samples with the different molar ratios of MnO_2 to ZrO_2 was measured at 200 °C under the adsorption conditions: [NO] = 2000 ppm, [O_2] = 5%, and the results are shown in Table 1. It reveals that the adsorption capacity of NOx increased with increasing the MnO_2 content in the sample, indicating that the Mn content significantly affects the maximum amount of NOx uptake. Kabin et al. [35] also evaluated the effects of different Ba loadings and Pt loadings [36] on NOx storage over a series of $Pt/BaO/Al_2O_3$ catalysts in both bench-scale monolith reactor and TAP (temporal analysis of products) reactor. They reported that the uptake of NO/NO_2 was closely related with Pt and BaO contents, and the optimal catalyst composition would depend on the operating conditions.

Table 1 shows that the maximum amount of NOx adsorbed is in good agreement with their BET surface areas, because high surface area can provide more active sites for the chemically adsorbed NOx species. The highest NOx uptake amount was available with 27.66 mg/g adsorbent on the 40% MnZr sample at 200 °C in the presence of oxygen. As compared with minor amount of NOx adsorbed on the samples without MnO_2 dopant (data not shown here) in the identical adsorption conditions, it is clear that Mn-containing species must play a key role for NOx adsorption. On the other hand, NO adsorption capacity was very small in the absence of O_2 at any conditions above, indicating that the NOx uptake was an adsorption–oxidation procedure. Considering these results, it is postulated that Mn species may help to oxidize NO into NO_2 or NO_3^- in the presence of oxygen, and the oxidized species are adsorbed on the samples. These results are consistent with other investigations. Eguchi et al. [29,30] verified that the NO absorption proceeds as the formation of nitrate stored on MnOx–ZrO_2 solid samples according to an infrared analysis of the absorbed species. The NOx adsorption on MnO_2/ZrO_2 and $Pt–MnO_2/ZrO_2$ catalysts is initiated by NO oxidation on the Mn or Pt surface, followed by NOx species oxidation. Similarly, Bentrup et al. [37] reported that manganese dioxide promoted the formation of nitrites and nitrates as main species of NO adsorption onto MnO_2/NaY through oxidation either by bulk oxygen or gaseous oxygen, as expressed by the processes $MnO_2 + NO \leftrightarrow MnO + NO_2$ and $MnO_2 + NO_2^- \leftrightarrow MnO + NO_3^-$, and the fixation of nitrates proceeds especially on cationic sites of the zeolite. This adsorption mechanism is possibly applied to explain the results obtained from the present investigation.

Table 1 also shows that the initial adsorption rate, hereafter defined as the average NOx uptake amount during the first 5 min. It was significantly high for the 40% MnZr sample; the exact reason was unknown currently. Practically, high adsorption rate is very useful for the adsorbent to be used in a quick-repeatedly adsorption–desorption cycles such as in lean burn engine exhaust treatments [19,31]. These saturated adsorbents can be completely regenerated by quickly raising temperature to 450 °C or higher as discussed later. Moreover, the adsorption/desorption was repeated more than 10 cycles without any remarkable deactivation.

For comparison, NOx adsorption on 40% MnZr-CP prepared by the co-precipitation method was also carried out at 200 °C under the same conditions as that for 40% MnZr. The result was also given in Fig. 3. It is observed that the maximum adsorption capacity of NOx at 200 °C was 16.89 mg/g adsorbent on 40% MnZr-CP, which was much lower than the value of 27.66 mg/g adsorbent on 40% MnZr sample. Therefore it seems essential that the high dispersion of Mn species on the surface area of MnO_2/ZrO_2 sample prepared by reverse microemulsion method could be responsible for the high amount of NOx uptake values on the sample [38].

Table 1
Adsorption characteristics of NOx on the MnO_2/ZrO_2 samples at 200 °C.

Sample	Mn/Zr (molar ratio)	BET surface area (m^2/g)	Maximum amount of NOx adsorbed at 100 min (mg/g adsorbent)	NOx initial adsorption rate[a] (mg/g adsorbent min)
2% MnZr	2:98	158	7.61	0.13
5% MnZr	5:95	181	16.08	0.69
15% MnZr	15:85	241	18.57	0.41
40% MnZr	40:60	256	27.66	2.63

[a] Average amount of NOx adsorbed per gram adsorbent per minute within first 5 min.

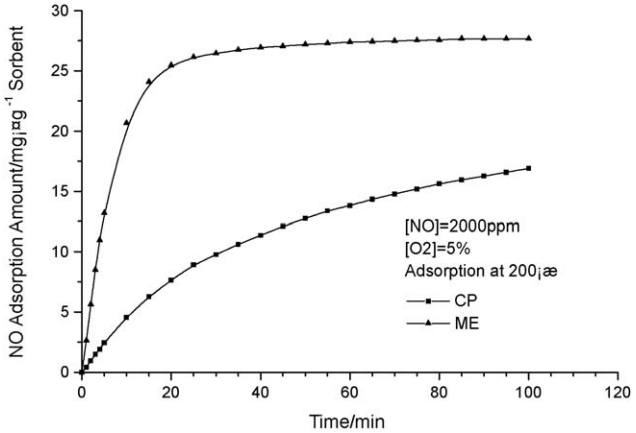

Fig. 3. Adsorption of NOx at 200 °C on 40% MnZr (ME) and 40% MnZr-CP (CP). Adsorption conditions: [NO] = 2000 ppm and [O_2] = 5%.

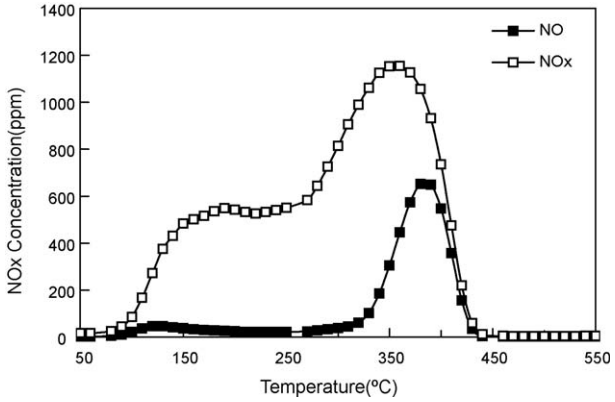

Fig. 4. TPD profiles of NOx (open symbols) and NO (solid symbols) on 40% MnO_2/ZrO_2 in argon under condition: the temperature rising rate: 10 °C/min; [NO] = 2000 ppm, [O_2] = 5% and adsorption time = 70 min.

TPD measurements of NOx and NO on the 40% MnZr solid in the inert or reducing gas stream were conducted to evaluate the effect of reducing agents on NOx desorption. Fig. 4 shows the TPD profiles of NOx desorption on 40% MnZr in a pure argon stream. The two peaks centered at ca. 170 °C and 350 °C may possibly be assigned to desorption of physically adsorbed NO_2 and nitrate species decomposition, respectively. In the NO-TPD profile, one high temperature peak centered at 375 °C was observed, which was assigned to desorption of strong adsorbed NO or nitrite species decomposition, because NO was favored for the thermodynamic equilibrium between NO and NO_2 at high temperatures [39]. Another low temperature peak at 140 °C is possibly due to physically adsorbed NO. When substituting argon with a reducing gas mixture of 0.6% CO/Ar (v/v), only one NO or NOx peaks could be detected as shown in Fig. 5, and the higher temperature peak in the TPD profile in Fig. 4 shifts to 210 °C in the presence of CO. The shift of the TPD peak temperature implies that CO addition may facilitate the nitrate species decomposition by CO reaction with the adsorbed nitrogen containing species, and hence benefits desorption of NO species at low temperatures, which is in line with the report on PdO–ZrO_2 [40]. Similarly, James et al. [41] also reported CO facilitating $Ba(NO_3)_2$ decomposition at lower temperatures. The result is possibly related to surface redox behaviours of the sample in the reducing gas streams.

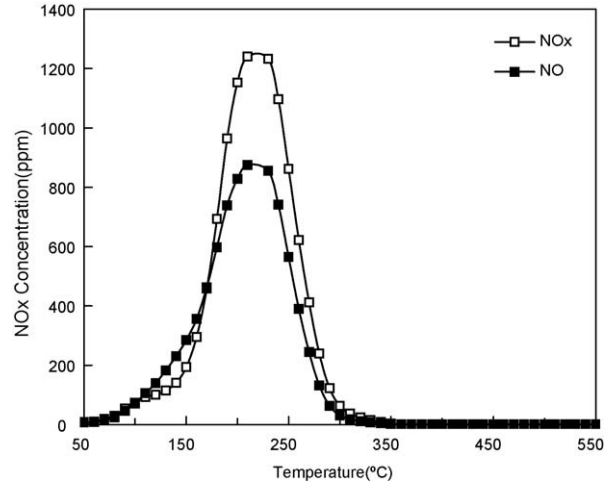

Fig. 5. TPD profiles of NOx (open symbols) and NO (solid symbols) on 40% MnO_2/ZrO_2 in argon stream in the presence of CO. Experimental condition: the temperature rising rate = 10 °C/min; [NO] = 2000 ppm, [O_2] = 5%, [CO] = 0.6% and adsorption time = 70 min.

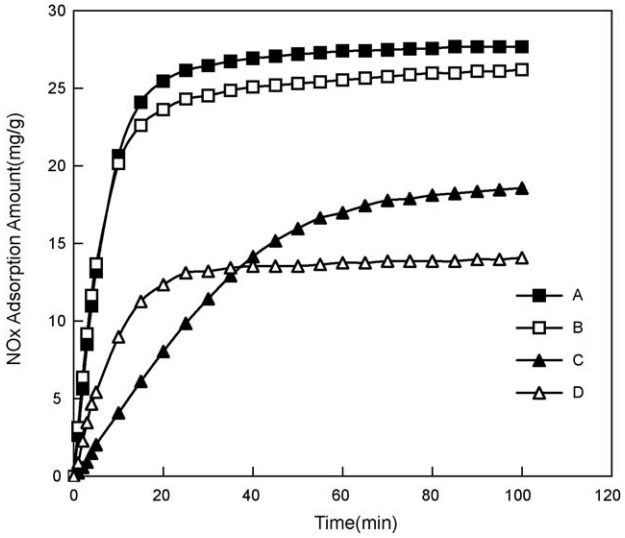

Fig. 6. Effect of pre-sulfation of various MnO_2–ZrO_2 samples on NOx adsorption: (A) 40% MnOx–ZrO_2; (B) sulfated 40% MnOx–ZrO_2; (C) 15% MnOx–ZrO_2; (D) sulfated 15% MnOx–ZrO_2. Adsorption conditions: [NO] = 2000 ppm, [O_2] = 5% and at 200 °C.

3.3. Effect of sulfur dioxide species

Sulfur dioxide derived from the burning of sulfur containing fuels is one of typical coexisting gasses with NOx, and it always causes strong deactivation for adsorbent materials [42], depending on their compositions [43]. Fig. 6 shows the effect of sulfur dioxide on the NOx adsorption over 15% MnO_2/ZrO_2 and 40% MnO_2/ZrO_2. After the sample was pretreated in a mixture of 300 ppm SO_2 and 5% O_2 to obtain the uptake amount of 0.2 wt% SO_4^{2-} on the 15% MnO_2/ZrO_2 sample, the maximum amount of NOx adsorption was decreased to 14.08 mg/g adsorbent at the time of 100 min on the sulfated sample as compared to the value of 18.57 mg/g adsorbent at 100 min on the 15% MnO_2/ZrO_2 sample without sulfation treatment. It shows a loss of approximately 24% of NOx adsorption capacity after sulfation, indicating that sulfur species competitively occupied a part of active adsorption sites for NOx species. Nevertheless, it was interesting to observe that the initial adsorption rate within the first 5 min for the sulfated sample was 1.08 mg/(g min), which was 2.6 times higher than the value of 0.41 mg/(g min) for the sample without sulfating. This finding is very useful for the practical application in a process of quick adsorption/desorption cycles. The exact reason is not completely understood up to now. Probably the sulfation modified the surface acidity and pore structures of the 15% MnO_2/ZrO_2 sample that results in a selective blockage of the material, and hence improving diffusion limitation of NOx species onto the sample. It is reported the NOx uptake rate is controlled by NOx adsorption to one or several type of sites [17,44] on the surface and active bulk components by NO diffusion through a barium nitrate layer to an underlying oxide or carbonate layer. Tuttlies et al. [45] attributed the two rate regimes to surface and bulk barium to the onset of diffusion limitations at the level of the barium particle for the Pt–BaO/Al_2O_3 system.

While under the similar sulfation condition, the maximum amount of NOx adsorption was only slightly decreased from 27.66 mg/g to 26.21 mg/g adsorbent at the time of 100 min on the 40% MnO_2/ZrO_2 sample after sulfation treatment. The maximal amount of adsorbed NOx was reduced by only 5% after sulfation. It is also shown that higher amount of manganese species on the adsorbent may gain sulfur tolerance to resist deactivation by sulfur poisoning. Note that both SO_2 and NOx are acidic species and they can be favorably adsorbed on a basic support, therefore

the acidity and basicity of the support will greatly affect their competitive adsorption on the adsorbent surface. It is well known that the surface acidity and basicity of ZrO_2 can be easily controlled by doping [46]. Takahashi et al. [47] reported that the acidity of ZrO_2–TiO_2 supports is an important factor influencing the sulfur tolerance of the NOx storage catalyst. Therefore, increasing manganese content in the Mn–Zr sample would modify the redox properties and surface acidity, and thus the NOx adsorption behaviours.

Xiao et al. [48] recently revealed that Mn-containing sample like $Mn/Ba/Al_2O_3$ is not sensitive to sulfur dioxide compared to $Pt/Ba/Al_2O_3$. Therefore, raising Mn loadings is in favor of resisting sulfur poisoning. On the other hand, Corbos et al. [26] showed that ZrO_2-containing materials were able to store NOx and presented an improved sulfur tolerance, and Luo and Gorte [49] showed that the oxidation and reduction of sulfate species on ceria and ceria–zirconia mixed oxides lead to an increase in the apparent "oxygen storage capacity" of sulfur-poisoned samples. Therefore it is likely that both MnOx and zirconia could be used to design sulfur-tolerant materials. It is reasonably proposed that a well-dispersed mixture of MnOx and ZrO_2 prepared by reverse microemulsions [38] was one of the alternative materials for NOx storage in the presence of sulfur species.

3.4. Effect of water vapor on NOx adsorption capacity

Water vapor usually coexists with NOx in the lean burn engine emissions or power plant emissions. The water vapor effect on the NOx adsorption over 15% MnZr is shown in Fig. 7. When the sample was first exposed to 2000 ppm NO and 2% O_2 at 25 °C in the absence of water vapor, two desorption peaks centered at 300 °C and 190 °C were observed in the TPD profile of NOx (Fig. 7A); similarly, two desorption peaks centered at 330 °C and 150 °C were found for the TPD profile of NO (Fig. 7B). However, in the presence of water vapor, only NO species can be detected in the desorption process. It was found that pre-adsorption of water vapor on the sample in 5% water vapor stream led to the high temperature desorption peak of NO shifting to a higher temperature position at 360 °C, and the low temperature peak remained almost unchanged; moreover a new peak appeared at 240 °C, indicating that water vapor may possibly modify the adsorbent surface in some way to produce a new kind of adsorptive sites. The similar shifting for the TPD peak position was also reported on $BaSnO_3$ [50]. By an in situ FT-IR technique, Bentrup [37] found a similar water effect on NOx adsorption over MnO_2/NaY. Pre-adsorbed water or greater amounts of water vapor in the feed hindered the NO adsorption by blocking the adsorption sites and resulted in nitrate formation at higher temperatures. Meanwhile, it is noted that the areas of both high and low temperature peaks were reduced simultaneously (Fig. 7C), which was due to the competitive adsorption between water vapor and NOx species. When the adsorption test was conducted in a gas mixture of 5% water vapor, 2000 ppm NO and 2% O_2 with argon as balance, the TPD peak positions were almost the same with those for pre-adsorption of H_2O, except the disappearance of the peak at 240 °C (Fig. 7D). Nevertheless, the intensity of the high temperature peak was reduced further, because of stronger competitive adsorption of water vapor on the sample compared to the case of first pre-exposing the sample to water vapor.

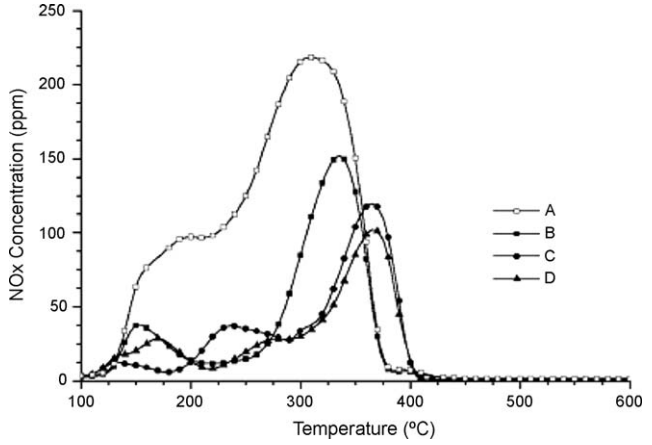

Fig. 7. TPD profiles of NOx (open symbols) or NO (solid symbols) on 15% MnO_2/ZrO_2 in argon at 25 °C after exposing to different gas streams: (A) 2000 ppm NO and 2% O_2; (B) 2000 ppm NO and 2% O_2; (C) 2000 ppm NO and 2% O_2 after exposing to 5% water vapor; (D) 2000 ppm NO, 2% O_2 and 5% H_2O.

There is a great number of literature reporting water effect for the typical $Pt–BaO/Al_2O_3$ materials. It is likely that water vapor is playing an important role in terms of the practical application of NOx storage techniques. Olsson et al. [51] and Scholz et al. [52] revealed that H_2O inhibited the NO oxidation capability of the Pt sites and no NO_2 formation was seen in the lean phase in the presence of H_2O, resulting in a decrease in NOx storage capacity. Regarding the $MnOx–ZrO_2$, probably the mechanism of water deactivation to NOx adsorption is similar with that in $Pt–BaO/Al_2O_3$ as discussed by Olsson et al. and Scholz et al. Further studies are necessary to determine the exact mechanism of water effect on the NOx storage performance on $MnO_2–ZrO_2$ materials over a wide range of adsorption conditions such as operating temperatures and water vapor concentrations.

4. Conclusion

A series of MnO_2/ZrO_2 mixed oxides with high surface areas were prepared in reverse microemulsions and tested for adsorption/desorption of NO in the presence of oxygen. The maximum amount of NOx adsorbed was increased with increasing MnO_2 content in the MnO_2/ZrO_2 samples. The significantly high uptake value of 18.57 mg/g adsorbent and 27.66 mg/g adsorbent was available at 200 °C on the 15% MnZr and the 40% MnZr samples, respectively. Addition of CO into the stream would facilitate the regeneration of the adsorbent materials at lower temperatures. Water vapor presence in the feed stream reduced the NOx adsorption capacity because of competitive adsorption with NOx species. It is noteworthy that a small amount of sulfur dioxide could increase the initial rate of NOx adsorption although it slightly decreased the maximum NOx adsorption capacity. The higher amount of manganese species on the MnO_2/ZrO_2 samples showed greater sulfur resistance in the adsorption of NOx and the maximum amount of adsorbed NOx was reduced by only 5% on the 40% MnO_2/ZrO_2 after its sulfating treatment. These results show that the MnO_2/ZrO_2 mixed oxides prepared in reverse microemusions may be potential adsorbents for the removal of NOx.

Acknowledgements

The financial supports by National Science Foundation of China (No. 29907003) and the National High-Tech Foundation (2001AA643030-1) are gratefully acknowledged.

References

[1] H. Bosch, F. Janssen, Catal. Today 2 (1988) 369.
[2] M.J. Izquirdo, B. Rubio, Environ. Sci. Technol. 32 (1998) 4017.
[3] K.C. Taylor, Catal. Rev. Sci. Eng. 35 (1993) 457.
[4] W. Bogner, M. Kramer, B. Krutzsch, S. Pischinger, D. Voigtlander, G. Wenninger, F. Wirbeleit, M.S. Brogan, R.J. Brisley, D.E. Webster, Appl. Catal. B 7 (1995) 153.
[5] M. Iwamoto, H. Hamada, Catal. Today 10 (1991) 57.

[6] V.I. Parvulescu, P. Grange, B. Delmon, Catal. Today 46 (1998) 233.
[7] R. Burch, T. Watling, Appl. Catal. B 17 (1998) 131.
[8] J.N. Armor, Appl. Catal. B 4 (1994) N18.
[9] E. Fridell, H. Persson, B. Westerberg, L. Olsson, M. Skoglundh, Catal. Lett. 66 (2000) 71.
[10] W.S. Epling, L.E. Campbell, A. Yezerets, N.W. Currier, J.E. Parks, Catal. Rev. Sci. Eng. 46 (2004) 163.
[11] A. Amberntsson, M. Skoglundh, S. Ljungstrom, E. Fridell, J. Catal. 217 (2003) 253.
[12] P. Engstrom, A. Amberntsson, M. Skoglundh, E. Fridell, G. Smedler, Appl. Catal. B: Environ. 22 (1999) L241.
[13] J. Dawody, M. Skoglundh, L. Olsson, E. Fridel, Appl. Catal. B 70 (2007) 179.
[14] H. Abdulhamid, E. Fridell, J. Dawody, M. Skoglundh, J. Catal. 241 (2006) 200.
[15] S. Elbouazzaoui, E.C. Corbos, X. Courtois, P. Marecot, D. Duprez, Appl. Catal. B 61 (2005) 236.
[16] F. Rohr, U. Gobel, P. Kattwinkeller, S. Philipp, P. Gelin, Appl. Catal. B 70 (2007) 189.
[17] W.S. Epling, G.C. Campbell, J.E. Parks, Catal. Lett. 90 (2003) 45.
[18] K. Lee, K. Watanable, M. Misono, Appl. Catal. B: Environ. 13 (1998) 141.
[19] M. Machida, K. Yasuoka, K. Eguchi, H. Arai, J. Chem. Soc., Chem. Commun. (1990) 1165.
[20] E. Fridell, M. Skoglundh, B. Westerberg, S. Johansson, G. Smedler, J. Catal. 183 (1999) 196.
[21] F. Rodrigues, L. Juste, C. Potvin, J.F. Tempere, G. Blanchard, G. Djega-Mariadassou, Catal. Lett. 72 (2000) 59.
[22] R.J. Hendershot, R. Vijay, C.M. Snively, J. Lauterbach, Appl. Surf. Sci. 252 (2006) 2588.
[23] I. Nova, L. Castoldi, L. Lietti, E. Tronconi, P. Forzatti, Catal. Today 2747 (2002) 1.
[24] S. Balcon, C. Potvin, L. Salin, J.F. Tempere, G. Djega-Mariadassou, Catal. Lett. 60 (1999) 39.
[25] A. Amberntsson, H. Persson, P. Engstrom, B. Kasemo, Appl. Catal. B: Environ. 31 (2001) 27.
[26] E.C. Corbos, X. Courtois, N. Bion, P. Marecot, D. Duprez, Appl. Catal. B 76 (2007) 357.
[27] M. Piacentini, M. Maciejewski, A. Baiker, Appl. Catal. B 66 (2006) 126.
[28] A.E. Palomares, A. Uzcátegui, A. Corma, Catal. Today 137 (2008) 261.
[29] K. Eguchi, M. Watabe, S. Ogata, H. Arai, J. Catal. 158 (1996) 420.
[30] K. Eguchi, T. Kondo, T. Hayashi, H. Arai, Appl. Catal. B: Environ. 16 (1998) 69.
[31] W.B. Li, R.T. Yang, K. Krist, J.R. Regalbuto, Energy Fuel 11 (1997) 428.
[32] R.T. Yang, W.B. Li, N. Chen, Appl. Catal. A: Gen. 169 (1998) 215.
[33] M.A. Copez-Quintela, J. Rivas, J. Colloids Interf. Sci. 158 (1993) 446.
[34] A.H. Heuer, L.K. Lenz, J. Am. Ceram. Soc. 65 (1982) C-192.
[35] K. Kabin, R. Muncrief, M.P. Harold, Y. Li, Chem. Eng. Sci. 59 (2004) 5319.
[36] K. Kabin, P. Khanna, R. Muncrief, V. Medhekar, M.P. Harold, Catal. Today 114 (2006) 72.
[37] U. Bentrup, Appl. Catal. B 32 (2001) 229.
[38] W.B. Li, W.B. Chu, M. Zhuang, J. Hua, Catal. Today 93–95 (2004) 205.
[39] K.H. Stern, J. Phys. Chem., Ref. Data 1 (3) (1972).
[40] M. Machida, A. Yoshii, T. Kijima, Int. J. Inorg. Mater. 2 (2000) 413.
[41] D. James, E. Fourre, M. Ishii, M. Bowker, Appl. Catal. B 45 (2003) 147.
[42] S. Matsumoto, Y. Ikeda, H. Suzuki, M. Ogai, N. Miyoshi, Appl. Catal. B 25 (2–3) (2000) 115.
[43] E.C. Corbos, X. Courtois, N. Bion, P. Marecot, D. Duprez, Appl. Catal. B 80 (2008) 62.
[44] K.S. Kabin, R.L. Muncrief, M.P. Harold, Catal. Today 96 (2004) 79.
[45] U. Tuttlies, V. Schmeisser, G. Eigenberger, Chem. Eng. Sci. 59 (2004) 4731.
[46] P.J. Moles, J. Adhes. Sci. Technol. 6 (1992) 61.
[47] N. Takahashi, A. Suda, I. Hachisuka, M. Sugiura, H. Sobukawa, H. Shinjoh, Appl. Catal. B 72 (2007) 187.
[48] J. Xiao, X. Li, S. Deng, F. Wang, L. Wang, Catal. Commun. 9 (2008) 563.
[49] T. Luo, R.J. Gorte, Appl. Catal. B 53 (2004) 77.
[50] S. Hodjati, C. Petit, V. Pitchon, A. Kiennemann, Appl. Catal. B 30 (2001) 247.
[51] L. Olsson, M. Abul-Milh, H. Karlsson, E. Jobson, P. Thormaehlen, A. Hinz, Topics Catal. 30/31 (2004) 85.
[52] C.M.L. Scholz, V.R. Gangwal, M.H.J.M. de Croon, J.C. Schouten, Appl. Catal. B 71 (2007) 143.